

Mechanisms underlying sequence-independent β -sheet formation

Chinlin Guo, Herbert Levine, Margaret S. Cheung

Department of Physics, University of California, San Diego

9500 Gilman Drive, La Jolla, CA 92093-0319

David A. Kessler

Department of Physics, Bar-Ilan University, Ramat-Gan, Israel

(Dated: December 2, 2024)

ABSTRACT

We investigate the formation of β -sheet structures in proteins without taking into account specific sequence-dependent hydrophobic interactions. To accomplish this, we introduce a model which explicitly incorporates both solvation effects and the angular dependence (on the protein backbone) of hydrogen bond formation. The thermodynamics of this model is studied by comparing the restricted partition functions obtained by “unfreezing” successively larger segments of the native β -sheet structure. Our results suggest that solvation dynamics together with the aforementioned angular dependence gives rise to a generic cooperativity in this class of systems; this result explains why pathological aggregates involving β -sheet cores can form from many different proteins. Our work provides the foundation for the construction of phenomenological models to investigate the competition between native folding and non-specific aggregation.

I. INTRODUCTION

β -sheets are an important element of protein structure, occurring often both in functional units and in pathological aggregates. For example, signaling proteins such as SH3 contain a β core. On the other hand, the precursors of amyloidogenesis are commonly found to have a β -sheet organization [1]; moreover, a conformational rearrangement can switch a functional β -sheet into an aggregation unit [2, 3]. As they play the role of stabilizing highly organized

architectures (either pathological or functional), β -sheets must be strongly cooperative units, responsible for lowering the free energy of these folded structures as compared to entropy-dominated more irregular patterns. This cooperativity refers to the fact that folding of a specific part of the overall structure will be aided by any contiguous folded regions; this allows there to be a sharp transition to a fully folded structure as these cooperative effects will compensate for the entropy loss. The origin of this cooperativity, however, has not been well characterized.

Typically it has been assumed that hydrophobic interactions are the origin of structural cooperativity [4]. This is because compared with the interactions between polar/charged side-chain groups (normally pairwise), the ones among hydrophobic groups have the advantage of many-body “collapsing” effects which eventually provide the system with a “long-range” coupling and hence a structural cooperativity. The straightforward implication of this line of reasoning is that a well-designed heterogeneous sequence is required to define a unique fold. This idea has been examined in a small β -sheet system, in which a hydrophobic force bridging three β strands (hence defined as a “long-ranged” coupling) was found necessary to stabilize the structure [5]. But, one can not ignore the evidence that some neurodegenerative diseases are caused by the aggregation of mutant proteins with long *hydrophilic* sequences (poly-glutamine in Huntington disease, e.g.,[6]); the β -sheet at the core of these aggregates are certainly not being stabilized by hydrophobic forces. This is consistent with recent experiments on small systems with purely hydrophilic sequences [7]. Together with the fact that most amyloidogenic precursors do not share any homologous sequence [1], it is therefore very likely that throughout a β -sheet architecture, short-ranged couplings provided by pairwise hydrogen-bond formation or polar/charged side-chain interactions, can be integrated into large-scale structural cooperativity so as to stabilize the system.

To study this issue, we introduce a new approach to constructing a tractable model of protein thermodynamics. The ingredients of this approach are a “co-plane” parameterization of the backbone degrees of freedom and an interaction potential which explicitly takes into account the solvation dynamics and the angular dependence of hydrogen-bond formation. The potential cooperativity is investigated by exploring the conditional probabilities of residues of being folded (i.e. in their native position and orientation) or unfolded depending on whether their neighbors are folded or unfolded [8]. Our results indicate that it is the de-solvation cavity formation and the hydrogen-bond angular dependence that provide

β -sheets with a systemic cooperativity. Since this property is sequence-independent, our results suggest why β -sheets can generically serve as the building blocks for constructing functional macromolecules, and why most functional proteins have the tendency to form aggregates at sufficiently high concentration.

II. METHOD

A. The model system

The system proposed here is based on the “ball-and-stick” model introduced in ref.[9]. In this approach, all NH, C $_{\alpha}$, CO (represented as C'), and C $_{\beta}$ side-chains are treated as “united” balls. The local backbone energy consists of a sum of terms: bond bending $V_{\theta} = \frac{1}{2} \sum k_{\theta}(\theta_i - \theta_0)^2$, dihedral rotations $V_{\omega} = \frac{1}{2} \sum \epsilon_{\omega}(1 + \cos \omega_i)$, $V_{\phi} = \frac{1}{2} \sum \epsilon_{\phi}(1 + \cos 3\phi_i)$, $V_{\psi} = \frac{1}{2} \sum \epsilon_{\psi}(1 + \cos 3\psi_i)$, and side-chain chirality $V_{\text{chiral}} = \sum \epsilon_{\text{chiral}} \Theta(\{[\hat{r}_{\text{NC}_{\alpha}} \times \hat{r}_{\text{C}_{\beta}\text{C}_{\alpha}}] \cdot \hat{r}_{\text{C}'\text{C}_{\alpha}}\}_i)$ summing over all i th components, with $\Theta(s) = (s + |s|)/2$. Here, since we are interested in sequence-independent effects, all side-chains are treated as polar (glutamine, e.g.) or weakly charged groups with homogeneous interactions that favor β -sheet formation. Also, we take the parameters $k_{\theta} = 200\text{kcal/mol} \cdot \text{rad}^2$, $\epsilon_{\omega} = 40\text{kcal/mol}$, $\epsilon_{\phi} = \epsilon_{\psi} = 0.45\text{kcal/mol}$, and $\epsilon_{\text{chiral}} = 10\text{kcal/mol}$ from [9].

B. The solvation force field

Next, we construct force fields for the non-local interactions. There is growing evidence that solvent effects play a significant role in protein folding and conformational changes [10, 11, 12, 13, 16]. We parameterize these effects implicitly (i.e. without including the water molecules explicitly) by designing a “double-well” potential that can account for contact formation and single-H $_2$ O hydration (within the contact pair); the barrier between the wells corresponds to the free energy cost involved in the transfer of a water molecule out of the hydration shell. Multiple shells could be accommodated in multiple-well potential, but this is not attempted here. The approximation of using an effective free-energy is justified via the observation that transfer of water from within the vicinity of contact pair is faster than the contact formation [10, 11, 12, 13].

There is no standard way to construct a continuous de/solvation potential [14] which can be used for Langevin simulations; we note that a recent Monte Carlo study [15] utilized a discrete version of such a potential. We therefore propose an empirical profile based on estimated experimental parameters. Specifically, we will take for H-bond formation

$$U_{\text{Hb}}(r) = \frac{A}{r^k} \left[\frac{1}{4r^{3k}} - \left(\frac{1}{(r_{\text{Hb}}^c)^k} + \frac{1}{(r_{\text{Hb}}^*)^k} + \frac{1}{(r_{\text{Hb}}^{\text{sol}})^k} \right) \frac{1}{3r^{2k}} \right. \\ \left. + \left[\left(\frac{1}{(r_{\text{Hb}}^c)^k} + \frac{1}{(r_{\text{Hb}}^*)^k} \right) \frac{1}{(r_{\text{Hb}}^{\text{sol}})^k} + \frac{1}{(r_{\text{Hb}}^c r_{\text{Hb}}^*)^k} \right] \frac{1}{2r^k} - \frac{1}{(r_{\text{Hb}}^c r_{\text{Hb}}^* r_{\text{Hb}}^{\text{sol}})^k} \right] \quad (1)$$

Here r is the distance between NH and CO, and the integer $k \in N$ ($k = 6$, e.g.) is chosen to give specific long-range behavior. The values $r = r_{\text{Hb}}^c$, $r = r_{\text{Hb}}^*$, and $r = r_{\text{Hb}}^{\text{sol}}$ represent the contact separation, the peak of the desolvation barrier, and the single intervening solvent molecule separation, respectively. Normally, $r_{\text{Hb}}^{\text{sol}}$ is obtained by adding the known value of r_{Hb}^c to the size of a single H_2O . A and r_{Hb}^* can be determined by the strengths of the H-bond [9] and the desolvation barrier; the latter is approximated by the surface energy involved in forming a desolvation cavity, estimated to equal $\sim 0.103\text{kcal}/(\text{mol } \text{\AA}^2)$ [13]. Here we have $r_{\text{Hb}}^c \approx 3.43 \text{\AA}$ and $r_{\text{Hb}}^* \approx 3.92 \text{\AA}$.

Clearly, the design principle of this type of formula is to have three roots for $dU_{\text{Hb}}(r)/dr = 0$ accounting for the desolvation barrier and for the two local minima; one can add more roots to address multiple solvation shell effects. Note that one might wish to “fine-tune” the potential profile more precisely (for instance, by being able to independently vary the width of the contact well). This can be accomplished by a more complicated expression (appendix A). Also, the strength of de/solvation might depend on the hydrophobicity of local environment [18] and one can certainly take this into account.

As discussed in [9, 17], hydrogen bond formation has a strong angular dependence on its surrounding backbone; thus, using the radial distance alone can not fully address the interaction. From fig.1(d), we note that such an angular dependence is merely the requirement that all atoms near to the interacting NH, CO (i.e. the shadowed area) are aligned “natively”. In [9], this “alignment” effect is accomplished by introducing artificial repulsive forces between H-bond neighbors. Here, we propose instead a “functional-block” (co-plane) scheme.

C. The co-plane approach

From fig.1(a), we notice that the peptide backbone between two contiguous C_α atoms has a “co-planar” structure because of the N-C-O bond resonance. This allows us to model the motion of a “co-plane” as a whole (i.e., with one dihedral angle ω fixed to $\approx 180^\circ$). The i^{th} co-plane is defined by three points $\{X_1^{(i)}, X_2^{(i)}, X_3^{(i)}\}$ where $X_1^{(i)}, X_3^{(i)}$ are simply the two C_α in the plane and $X_2^{(i)}$ is a virtual point satisfying $\overrightarrow{X_1^{(i)}X_2^{(i)}} \perp \overrightarrow{X_2^{(i)}X_3^{(i)}}$, fig.1(b). Once the degree of freedom corresponding to this point is specified, all the atomic locations of the amide and carbonyl groups are fixed. Note that a convenient way to define the arbitrary point X_2 is such that the vector $\overrightarrow{X_2^{(i)}X_3^{(i)}}$ points directly at the C_α of the neighboring strand if the system is in the native β -sheet structure; see fig.1(c). Once $X_2^{(i)}$ is chosen, this determines the in-plane angles θ_1 and θ_2 as well as the virtual plane projection angle θ_3 . We computed all these objects by using the native value of bond angles [9] and dihedral angles observed in regular β -sheets ($\phi \sim -138 \pm 1^\circ$, $\psi \sim 135 \pm 1^\circ$) [17]. This leads to all geometrical properties of the virtual plane, including $\theta_1 = 64.7^\circ$, $\theta_2 = 62.2^\circ$, $\theta_3 = 22.4^\circ$, $\overline{X_1X_2} = 3.75 \text{ \AA}$, $\overline{X_2X_3} = 0.57 \text{ \AA}$.

Given the native plane, we define the range of possible non-native structures via allowing the orientation of the planes to vary. This yields three degrees of freedom per residue; two reflect the angles needed to define the direction of the fixed length vector going from one C_α to the next while the third refers to a rolling of the plane around this vector. One can then work out the geometrical problem of expressing, in terms of these degrees of freedom, the residual terms in the backbone energy arising from the dihedral terms involving ϕ and ψ , the bending of the bond angle $\angle C'C_\alpha N$, and the side-chain chiralities between consecutive blocks. Our approach fully maintains the overall translation and rotational degrees of freedom of the protein molecule. This co-plane parameterization greatly reduces our computation effort as compared to all atom backbones, yet maintains the roll degree of freedom not present in the simplified C_α model. As will be shown later, this degree of freedom is important for the study of β -sheet cooperativity.

D. The structural factor

Now we use the co-plane approach to model the H-bond angular dependence. From fig.1(e), we note that having a H-bond between blocks i, j requires fixing two rotational and two translational degrees of freedom. More precisely, we need $\overrightarrow{X_1^{(i)}X_2^{(i)}}$ antiparallel to $\overrightarrow{X_1^{(j)}X_2^{(j)}}$, and $\overrightarrow{X_2^{(i)}X_3^{(i)}}$ parallel to $\overrightarrow{X_2^{(j)}X_3^{(j)}}$, whereas for translational alignment, the two sets of points $\{X_1^{(i)}, X_2^{(j)}, X_3^{(j)}\}$ and $\{X_1^{(j)}, X_3^{(i)}, X_2^{(i)}\}$ must be collinear. This leads us to define a “structural form factor” that monitors the “angular nativeness” in the H-bond;

$$x_{\text{Hb}}^{(i,j)} = \frac{1}{16} \left[1 - \widehat{X_{12}^{(i)}} \cdot \widehat{X_{12}^{(j)}} \right] \left[1 + \widehat{X_{23}^{(i)}} \cdot \widehat{X_{23}^{(j)}} \right] \times \left[1 + \cos \angle X_2^{(j)} X_1^{(i)} X_3^{(j)} \right] \left[1 + \cos \angle X_2^{(i)} X_1^{(j)} X_3^{(i)} \right] \quad (2)$$

where $\widehat{X_{ab}^{(k)}}$ is the unit vector connecting $X_a^{(k)}, X_b^{(k)}$. Note that $x_{\text{Hb}}^{(i,j)}$ has maximum of 1 only when all the alignment criteria are satisfied.

We now wish to incorporate this form factor into the Hamiltonian in such a manner as to ensure that at small x_{Hb} , the two interacting blocks are unlikely to form H-bond. A simple phenomenological way to proceed is to introduce a potential profile which has two parameters dynamically modulated by x_{Hb} with a fixed solvation energy E_{sol}

$$U_{\text{Hb}}(r, x_{\text{Hb}}) = \frac{A(x_{\text{Hb}})}{r^k} \left[\frac{1}{4r^{3k}} - \left(\frac{1}{r_{\text{Hb}}^x k} + \frac{1}{(r_{\text{Hb}}^*)^k} + \frac{1}{(r_{\text{Hb}}^{\text{sol}})^k} \right) \frac{1}{3r^{2k}} \right. \\ \left. + \left[\left(\frac{1}{r_{\text{Hb}}^x k} + \frac{1}{(r_{\text{Hb}}^*)^k} \right) \frac{1}{(r_{\text{Hb}}^{\text{sol}})^k} + \frac{1}{(r_{\text{Hb}}^x r_{\text{Hb}}^*)^k} \right] \frac{1}{2r^k} - \frac{1}{(r_{\text{Hb}}^x r_{\text{Hb}}^* r_{\text{Hb}}^{\text{sol}})^k} \right] \quad (3)$$

Here the first dynamical parameter $A(x_{\text{Hb}})$ is determined by fixing $U_{\text{Hb}}(r_{\text{Hb}}^{\text{sol}}, x_{\text{Hb}}) = E_{\text{sol}}$ and for another parameter, we have used a linear relation $r_{\text{Hb}}^x = x_{\text{Hb}} r_{\text{Hb}}^c + (1 - x_{\text{Hb}}) r_{\text{Hb}}^*$. Examples of this modulated double-well profile are shown in fig.2(a).

Aside from NH–OC hydrogen bond, we include in our model bonding between $C_\alpha\text{-H}\cdots\text{O}=\text{C}$ [19] and also side-chain interactions [8]. These interactions have a strong chirality [9] and an angular dependence that involves at least two contiguous blocks. From fig.1(d), we note that the native configuration for interacting consecutive blocks $i, i + 1$ and $j, j + 1$ (here $i(j) + 1$ is the block next to $i(j)$ along the same strand) requires $\widehat{X_{23}^{(i)}} (\widehat{X_{23}^{(j)}})$ antiparallel to $\widehat{X_{23}^{(i+1)}} (\widehat{X_{23}^{(j+1)}})$. Therefore, in analogy to the aforementioned H-bond, we propose a structural factor for these additional interactions

$$x_{\text{chiral}}^{(i,j)} = \frac{1}{4} x_{\text{Hb}}^{(i,j)} x_{\text{Hb}}^{(i+1,j+1)} \left[1 - \widehat{X_{23}^{(i)}} \cdot \widehat{X_{23}^{(i+1)}} \right] \left[1 - \widehat{X_{23}^{(j)}} \cdot \widehat{X_{23}^{(j+1)}} \right] \quad (4)$$

with an interaction potential either $U_{\text{sc}}(r, x_{\text{chiral}})$ or $U_{\text{C}_\alpha\text{H-OC}}(r, x_{\text{chiral}})$ taken to be similar to $U_{\text{Hb}}(r, x_{\text{Hb}})$. We use a side-chain interaction strength in the range $-0.1 \sim -2.0$ kcal/mol[4, 17], and the strength of $\text{C}_\alpha\text{-H} \cdots \text{O}=\text{C}$ interaction is taken to be half that of a single H-bond [19].

E. The local melting approach

Our approach is based on the concept of exploring the system cooperativity by studying partially folded structures[8]. Specifically, we investigated two cases; first, the ensemble that has all blocks frozen in their folded configurations aside from either a) a few blocks at the end of one of a strand or b) a few blocks buried inside the sheet. Since there is no long-ranged interaction, we assume that the “local” thermodynamics of specified blocks will not be affected significantly by the dynamics of very distant blocks. This allows us to compute a “conditional” partition function in which, except for those specified blocks, the rest can be treated as frozen. Since we are interested in studying how native structure of some parts of the architecture bias the rest of the folding thermodynamics, we take these frozen blocks to be in their native positions.

If the number of molten blocks n is small, one can get the “local” partition function by explicit numerical integration. For instance, in single-block β -tail case, the partition function reads $\int dX_2 dX_3 \delta(\overline{X_1 X_2} - \overline{X_1 X_2}^N) \delta(\overline{X_2 X_3} - \overline{X_2 X_3}^N) e^{-H/k_B T}$ where $\overline{X_1 X_2}^N = 3.75 \text{ \AA}$, $\overline{X_2 X_3}^N = 0.57 \text{ \AA}$ are the native constants. Then, because of the δ functions, the partition function is reduced to an integral over three angles defining the orientation of the last plane. If n is large, on other hand, we use instead a standard Langevin simulation method [8, 9].

F. The role of the force field

To characterize the roles of structural factors and solvation effects in β -sheet formation, we have studied four different force fields. Two of these rely on the $\text{G}\bar{\text{o}}$ approach of allowing hydrogen bond formation only between those residues that have such an interaction in the native structure. These are **(A) LJ^{G $\bar{\text{o}}$}** : $U_{\text{LJ}}^{\text{G}\bar{\text{o}}}(r) = |E_{\text{Hb}}| \frac{(r_{\text{Hb}}^c)^6}{r^6} \left[\frac{(r_{\text{Hb}}^c)^6}{r^6} - 2 \right]$, $\text{G}\bar{\text{o}}$ -typed L-J potential. **(B) Solv^{G $\bar{\text{o}}$}** : $U_{\text{Solv}}^{\text{G}\bar{\text{o}}}(r) \Rightarrow \text{eqn.(1)}$, $\text{G}\bar{\text{o}}$ -typed potential with de/solvation effect. Now, the entire justification of this approach is absent in systems with homoge-

neous systems such as the ones of primary concern here, but it is still worthwhile comparing the results of our proposed form-factor model with these alternatives. The third force field is taken to be **(C) LJ^{ang}**: $U_{LJ}^{ang}(r) = A_{LJ}(x_{Hb}) \frac{[r_{LJ}(x_{Hb})]^6}{r^6} \left[\frac{[r_{LJ}(x_{Hb})]^6}{r^6} - 2 \right]$, a 2-dynamical-parameter L-J potential with our proposed angular dependence. This profile is designed to help distinguish the effects of solvation and structural factors. Thus, except for the absence of a desolvation barrier, this potential is quite similar to the solvation one, eqn.(3). Explicitly, we let a non-native alignment factor $x_{Hb} < 1$ give rise to a linear shift $|U_{LJ}^{ang}(r_{LJ}(x_{Hb}))| = A_{LJ}(x_{Hb}) = x_{Hb}|E_{Hb}| + (1 - x_{Hb})|E^{sol}|$ for the first parameter. Also, to achieve a repulsive effect similar to that in eqn.(3), we set $U_{LJ}^{ang}(r_{Hb}^x) = U_{Hb}(r_{Hb}^x, x_{Hb})$, i.e., $r_{LJ}(x_{Hb}) = r_{Hb}^x (1 + \sqrt{1 + U_{Hb}(r_{Hb}^x, x_{Hb})/A_{LJ}(x_{Hb})})^{1/6}$ for the second parameter. Fig.2(b) shows the modulation of this force field due to varying of structural factor. Finally, our full model is **(D) Solv^{ang}**: $U_{Solv}^{ang}(r) \Rightarrow$ eqn.(3), the de/solvation potential with the proposed angular dependence.

III. RESULTS

In this section, we present results of some preliminary calculations based on our modeling scheme. First, we focus on unfreezing small numbers of blocks so as to investigate the differences between the different force field choices. The conclusion of these studies is that the solvation model with the angular factor modulation does capture the type of behavior we wish to preserve from the full (all-atom) system. Afterwards, we study a large dynamical block with this model and demonstrate that solvation must occur as a cooperative process involving many residues simultaneously.

For small blocks, we use exact numerical integration of the partition function to study the relative probabilities of different arrangements of the unfrozen blocks. Fig.3,4 presents these results for the different force fields. Let us first discuss the single-block β -tail case, fig.3. For this situation, the maximum possible NH \cdots OC distance as determined by the range of integration, is smaller than that is necessary to fit a water molecule in between and thus there cannot be any true secondary solvated minimum. We do see however the fact that having the solvation barrier and (to a lesser extent) the angular factors make a big difference in the relative probabilities of NH \cdots OC interacting distance (i.e., H-bond separation between the mobile block and its native partner). Specifically, there is no hint of

well-separated 2-state behavior for the $G\bar{o}$ -type Lennard-Jones potential ($LJ^{G\bar{o}}$). However, a small barrier appears if the potential has an angular dependence (in LJ^{ang}), and becomes significant if solvation effects are included (in $Solv^{G\bar{o}}$, $Solv^{ang}$).

It is interesting to notice that the barrier for $Solv^{G\bar{o}}$ potential is much larger than that of $Solv^{ang}$ one. This is because the desolvation barrier height is fixed in the former case, but modulated (by the angular factor) in the latter one. We note that because of the bond angle $\angle C' C_\alpha N$ potential, the pdf of H-bond separation is concentrated on the “ring” that satisfies $\angle C' C_\alpha N = \angle C' C_\alpha N_{native}$. On this ring, only a few “points” will give minimal dihedral angle (ψ, ϕ) energies. These points correspond to the sharp, tiny peaks in fig.3 that have free energy difference $\approx \epsilon_\psi + \epsilon_\phi \approx 1\text{kcal/mol}$ from their neighborhood; if we reduce the bond angle stiffness k_θ , these sharp peaks became more broadened (data not shown). Note that this effect comes from the backbone energy and is independent of the choice of non-local interactions.

Next, we studied the pdf (probability distribution function) of n -block “buried” cases. For small n , the configurations are clearly constrained to a great extent by the fixed neighbors. For $n = 1$, there is neither 2-state behavior nor any qualitative difference among the pdf of the different force fields (data not shown). All significant probability is confined in the H-bond well, indicating a strong topological confinement to force the folding of a single unfolded block buried amidst folded ones. When $n = 2$, we still do not have enough freedom of backbone motion to allow for a solvated second minimum for the main Hydrogen bond; the maximum separation is slightly above 4.1 \AA . Nonetheless, we see clear differences between the different force field choices. For the simplest $LJ^{G\bar{o}}$ model, there is no confinement to a narrow contact well. Adding the angular factor back in, we create a barrier as the distance is increased. This barrier is due to the modulation of the LJ potential by the angular factor, making it repulsive if the orientation is not properly matched. Alternatively, adding the solvation effect as in $Solv^{G\bar{o}}$ also introduces a barrier; this is because rolling of the co-plane allows for a wide separation (and hence going up and down the solvation barrier) in the $C_\alpha H-OC$ and side-chain–side-chain interactions. Finally, putting both effects in leads to a very large degree of confinement in the main well. This result suggests that the system cooperativity is enhanced by both structural and solvation effects such that an unfolded molten block is strongly biased to fold if caged by folded ones.

To further characterize the difference between the varying choices of force fields, we

computed (in the 2-block buried case) the conditional distribution function of one molten block with respect to the un/folding state of another (defined as if its H-bond separation $r_2 \gtrless r_{\text{Hb}}^*$), $P(r_1|r_2 > r_{\text{Hb}}^*)$, $P(r_1|r_2 < r_{\text{Hb}}^*)$, where r_1 , r_2 are the H-bond separations of these two blocks. In principle, if the system has a collective behavior, un/folding of one block should force the un/folding of another, implying a well-separated $P(r_1|r_2 \gtrless r_{\text{Hb}}^*)$. In fig.4(b), however, we found that $P(r_1|r_2 \gtrless r_{\text{Hb}}^*)$ are well separated only for the force field having both angular and solvation effects (Sol^{ang}). Note that it is important to realize that the separated probability peaks have been separately normalized; the actual probability for being at the larger distance is extremely small as is evident from the previous figure. Finally, it is crucial to understand that it is not the actual distance separation in the figure which is important - this separation is quite small. Instead, the two peaks correspond to either having the full Hydrogen bond energy (by satisfying *both* the distance and angular conditions) or not having that energy. The right hand distribution does not have the contact energy as it forced into an unfolded angular configuration by having an unfolded neighbor. The separation of conditional probability distributions is much clear if plotted on the variation of H-bond energy E_1 of one block, i.e., $P(E_1(r_1)|r_2 > r_{\text{Hb}}^*)$, $P(E_1(r_1)|r_2 < r_{\text{Hb}}^*)$, fig.4(b), in which we see that only the full model LJ^{ang} has the best separation effect. Note that the distribution $P(E_1(r_1)|r_2 < r_{\text{Hb}}^*)$ has a partial H-bond formation; this comes from the coupling of its caged neighbor.

The conclusion from these small block studies is that the full model being proposed here leads to strong correlations between the behaviors of neighboring blocks. For the system as a whole, this should mean that complicated configurations with repeated “interfaces” between unfolded and folded residues should be strongly suppressed in favor of simpler configurations with large patches of residues being either all in contact or all not in contact.

To see this explicitly, we turn to a Langevin simulation of a ten-block buried case. Because of the large barrier needed to melt the blocks, we set the simulation temperature far beyond the physiological range. From fig.5(a) (using Sol^{ang}), we note that the pdf of native H-bond distances are well separated by the H-bond desolvation barrier. Interestingly, we note that even though they are governed by a fixed desolvation potential, the un/folding barrier for each molten block is not quite the same. As the monitored block is taken to lie closer to the confined ones, its distribution function (the free energy well $-k_B T \ln P(r)$) in the non-H-bond-formation region (disordered phase) becomes less deep, manifesting a

stronger folding bias for any unfolded residues near those folded ones. On the other hand, we noticed a progressive increase of the barrier separating ordered (in the H-bond contact well) and disordered phases for residues away from the confined region. That is, once there are many free residues, the probability of being in some intermediate state is greatly suppressed compared to all being folded or all being unfolded. The barrier can be thought of as being due to a collective water expelling process for those monitored blocks away from confined region (i.e., with more mobile neighbors), or vice versa, a manifestation of collective re-solvation kinetics. Some snapshots of the kinetics are shown fig.5(b).

IV. DISCUSSION

We have explored the microscopic cooperativity in a homogeneous β -sheet system, with different choices for the force fields. The one exhibiting the most cooperativity is a new contact potential that we constructed so as to include de/solvation effects. Also, instead of simulating all backbone atoms or a simplified C_α model, a functional block (co-plane) approach was proposed. This approach greatly reduces our computational effort; however, it still keeps the right angular degrees of freedom (missing in C_α model) and gives rise to a structural form factor that helps account for β -sheet cooperativity.

Using our proposed structural factor, we then can fully describe the angular dependence of contact formation. To elucidate the local thermodynamics and system cooperativity, a “local melting” method has been introduced. This method can be further used to explore local nucleation or de-solvation events in any system lacking long-ranged spatial couplings. Our results suggest that in the absence of such long-ranged interactions, the β -sheet cooperativity arises from both the structural factor (contact angular dependence) and protein de/solvation effects. Neither a Lennard-Jones nor G \bar{o} -typed interaction can quite reproduce this property. Since this phenomenon is sequence-independent, the results can be considered to apply in general to β -sheet structures.

In previous studies [8], we have argued that having a structural cooperativity requires many-body effects and the essential part is an entropic penalty in partially folded structures rather than side-chain interactions. Of course, one possible source of such a many-body effect is dihedral confinement via the corresponding terms in the backbone energy. As illustrated in our study, when the system is close to fully folded state, the backbone topological (through

dihedral/bond angles) confinements are strong enough to complete the folding. However, when the system has larger unfolded structure, the magnitude of this type of interaction, is too small to generate a strong system cooperativity, as shown by our findings for the pure G \bar{o} -typed Lennard-Jones potential case. Instead, this is the role of the angular dependence which integrates the contact strength into the backbone Hamiltonian and thus amplifies the confinement. This leads to a competition with solvation dynamics; in other words, when the solvent tries to pull the interacting blocks apart, the confining force amplified by folded neighbors can hold them back. Consequently, in a partially folded structure, any small regions of unfolded blocks caged by folded ones are thermodynamically unfavorable and will be forced to fold or will unzip the folded ones [8].

Given our results, the existence of macroscopic cooperativity in such an architecture would not be surprising. Indeed, from a physics prospective, the consecutive H-bond formation in a planar β -sheet resembles a 2-dimensional system with cooperative short-ranged interactions. One recalls that such an architecture can have 2-state-like behavior at certain system sizes. Thus, while there has been a concentration of effort on understanding the role the sequence heterogeneity for protein folding and design, we would like to point out that this generic cooperativity buried in the β -sheet architecture can also serve as a “building block” to construct macromolecular structure. However, this same building block can also provides the mechanism for pathological aggregation.

Then, what would be the physiological role and evolutionary principle of having sequence heterogeneity, in the presence of possible β -architectures? Certainly, with the fast time scale (of order of 0.1 ns, estimated from our Langevin simulations) for a single C $_{\alpha}$ block folding, any pre-folded β -architecture with ordered, exposed amide and carbonyl oxygen could lead to a seeding process and non-specifically precipitate surrounding unfolded peptides; this has been observed in the elongation process of amyloidogenesis [3]. The physiological role of heterogeneity, therefore, would be to distort the orientation of exposed amide and carbonyl groups into non-aggregation competent form. Indeed, this idea has been verified in a recent tryptophan zipper model [20]. Exploring the competition between native folding due to specific sequence heterogeneity and pathological aggregation due to generic cooperativity is perhaps the most important direction for future study.

As a side point, we have introduced an approach to de/solvation which can be used directly for Langevin simulations. It has been noticed that the (de)-solvation effects are

important in protein folding and functioning, but no standard model has been proposed [10, 11, 12, 13, 14, 16]. Also, we note that solvent dynamics can be regulated by system hydrostatic pressure [10]. Interestingly, many adhesion and hemostasis-related proteins are very sensitive to shear stress and pressure change; perhaps a local de/re-solvation event might trigger a cooperative conformational change which ultimately has large scale consequences [16]. Thus, microscopic cooperativity can be amplified into a macroscopic response; this also needs to be explored in future work.

APPENDIX A: MODIFIED DESOLVATION POTENTIAL

The simplified double-well potential provides the basic insight on how de/solvation effect involves in protein cooperativity. However, one might wish to modify this model to include more control parameters. For instance, we might design

$$U_{\text{HB}}(r) = \begin{cases} -B \frac{(r-r_1)^2 - h_1}{(r-r_1)^{2m} + h_2} & \text{if } r > r_{x1}, \\ Ay(r) \{[y(r)]^2 + b\} + U_{\text{HB}}(r_{x1}) & \text{if } r \leq r_{x1} \\ \text{with } \begin{cases} y(r) = \frac{z(r)[z(r)-1]}{z(r)+s}, \\ z(r) = \frac{r_{x1}/r-1}{r_{x1}/r_{x0}-1} \end{cases} \end{cases}$$

and r as the distance between NH and CO, fig.1(a). Here, the interacting distance for formation of contact, desolvation barrier, and single-solvent separation are $r = r_0$, $r = r_1$, $r = r_2$, with free energy amplitude D_0 , D_1 , D_2 , respectively, and the width of the contact well is controlled by the span between $r = r_{x0}$ and $r = r_{x1}$. Normally, r_2 is separated from r_0 by the size of a single water molecule. The integer $m > 2$, on the other hand, is chosen for the long-distance behavior, and the six unknowns B, h_1, h_2, A, b, s can be determined by D_0, D_1, D_2, r_0, r_2 and one continuity requirement (dU_{HB}/dr at $r = r_{x1}$). Using this model, one has a complete control on the potential profile (the well width for the contact entropy, e.g.).

[1] M. Sunde, L.C. Serpell, M. Bartlam, P.E. Fraser, M.B. Pepys, and C.C. Blake, J. Mol. Biol. **273**, 729 (1997).

- [2] K. Liu, H.S. Cho, H.A. Lashuel, J.W. Kelly, and D.E. Wemmer, *Nat. Struc. Biol.* **7**, 754 (2000).
- [3] J.W. Kelly, *Nat. Struc. Biol.* **7**, 824 (2000).
- [4] A. Fersht, in *Structure and mechanism in protein science*. (W.H. Freeman & Company. New York, 1999) Chapter 17.
- [5] T. Kortemme, M. Ramirez-Alvarado, and L. Serrano, *Science* **281**, 253 (1998).
- [6] M.F. Perutz, T. Johnson, M. Suzuki, and J.T. Finch, *Proc. Natl. Acad. Sci. USA.* **91**, 5355 (1994).
- [7] S. Koide, X. Huang, K. Link, A. Koide, Z. Bu, and D.M. Engelman, *Nature* **403**, 456 (2000).
- [8] CL. Guo, H. Levine, and D.A. Kessler, *Phys. Rev. Lett.* **84**, 3490 (2000); *Proc. Natl. Acad. Sci. USA.* **97**, 10775 (2000).
- [9] S. Takada, Z. Luthey-Schulten, and P.G. Wolynes, *J. Chem. Phys.* **110**, 11616 (1999).
- [10] G. Hummer, S. Garde, A.E. Garcia, M.E. Paulaitis, and L.R. Pratt, *Proc. Natl. Acad. Sci. USA.* **95**, 1552 (1998).
- [11] A.E. Garcia and G. Hummer, *Protein: Structure, Function, & Genetics.* **38**, 261 (2000).
- [12] J.D. Dunitz, *Science* **264**, 670 (1997).
- [13] H.S. Ashbaugh, E.W. Kaler, and M.E. Paulaitis, *J. Am. Chem. Soc.* **121**, 9243 (1999).
- [14] B. Roux, and T. Simonson, *Biophys. Chem.* **78**, 1 (1999).
- [15] N. Helson, J.N. Onuchic, and A.E. Garcia, *Proc. Natl. Acad. Sci. USA.* **96**, 14848 (1999).
- [16] R. Celikel, Z.M. Ruggeri, and K.I. Varughese, *Nat. Struc. Biol.* **7**, 881 (2000); P. Marchese, E. Saldivar, J. Ware, and Z.M. Ruggeri, *Proc. Natl. Acad. Sci. USA.* **96**, 7837 (1999).
- [17] T.E. Creighton, in *Proteins: structure and molecular properties* (W.H. Freeman and Company. New York. 1996) Chapter 4 & 5.
- [18] K. Lum, D. Chandler, and J.D. Weeks, *J. Phys. Chem.* **103**, 4570 (1999).
- [19] R. Vargas, J. Garza, D.A. Dixon, B.P. Hay, *J. Am. Chem. Soc.* **122**, 4750 (2000).
- [20] A.G. Cochran, N.J. Skelton, and M.A. Starovasnik, *Protein Science* **9**, suppl.1 165 (2000).

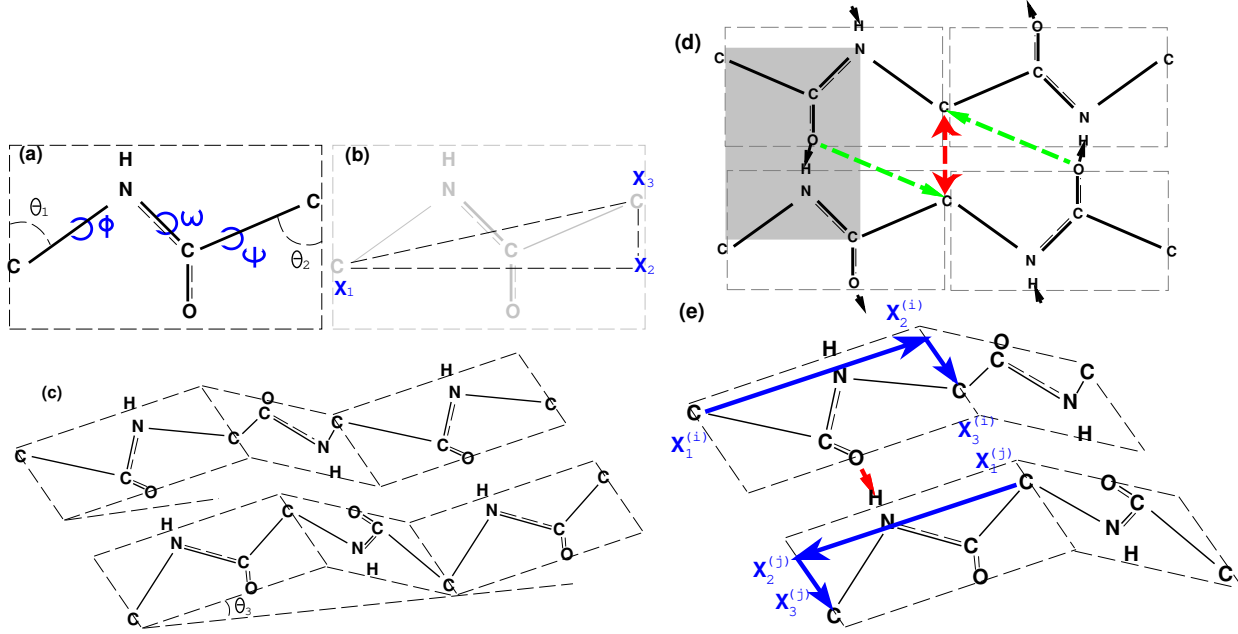


FIG. 1: (a) The co-planar structure with (b) the three virtual points $\{X_1, X_2, X_3\}$ and dihedral angles ω, ϕ, ψ labeled. The virtual bond lengths and angles are determined so as to give (c) a regular, symmetric β -sheet structure with side-chains and $C_\alpha H$ bonds alternately pointing up and down (not drawn here) periodically. (d) The side-chain and $C_\alpha H-OC$ interactions are indicated by red, green arrows, respectively, with the shadowed area indicating the atoms involved determining the angular dependence of a single H-bond. (e) If two interacting blocks i, j are to have a native H-bond (the red arrow), proper alignment of two pairs of planar vectors and collinearity of the two sets of points $(X_1^{(i)}, X_2^{(i)}, X_3^{(i)}; X_1^{(j)}, X_2^{(j)}, X_3^{(j)})$ are required.

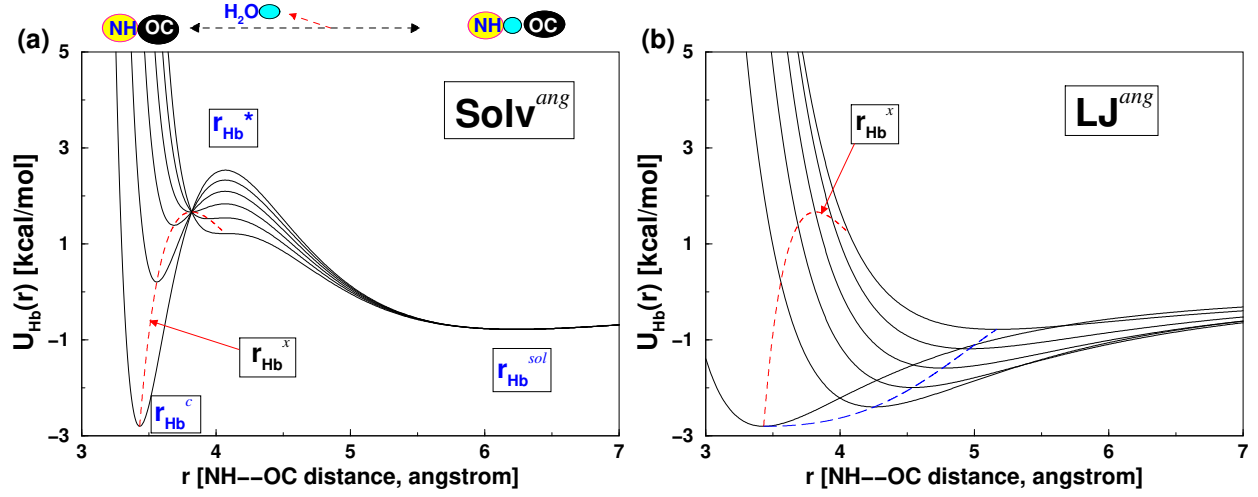


FIG. 2: The structural-factor-dependent H-bond potential profiles in units of kcal/mol with interaction distance r (NH \cdots CO) measured in \AA . (a) The (de)-solvation force field $U_{\text{Hb}}(r, x_{\text{Hb}})$. The barrier height between $r = r_{\text{Hb}}^*$ and the solvent-separated minimum ($r = r_{\text{Hb}}^{\text{sol}}$) represents the free energy cost in desolvation cavity formation. Here we have graphed $U_{\text{Hb}}(r, x_{\text{Hb}})$ from $x_{\text{Hb}} = 0$ to 1. The red dashed curve represents the modulation of the contact minimum ($r_{\text{Hb}}^x, U_{\text{Hb}}(r_{\text{Hb}}^x, x_{\text{Hb}})$). (b) The Lennard-Jones force field $U_{\text{LJ}}^{\text{ang}}(r)$, where the profile is modulated by changing the contact minimum (blue curve) $|U_{\text{LJ}}^{\text{ang}}(r_{\text{LJ}}(x_{\text{Hb}}))| = x_{\text{Hb}}|E_{\text{Hb}}| + (1 - x_{\text{Hb}})|E^{\text{sol}}|$ from the H-bond contact energy E_{Hb} to the single H₂O hydration E^{sol} . The major difference between (a) and (b) is the desolvation barrier.

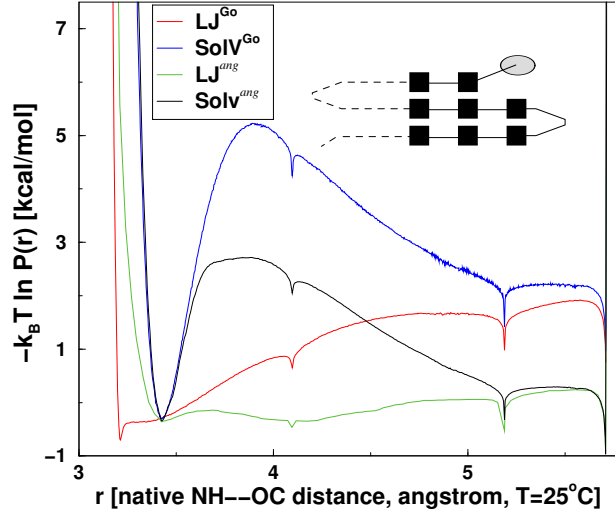


FIG. 3: The numerical results for the probability distribution function (pdf) $P(r)$ of $\text{NH}\cdots\text{OC}$ separation r of the “molten” block respective to its native partner in the β -tail single-block case (indicated in the inserted diagram; black: frozen, gray: mobile). Here $\text{LJ}^{\text{G}\bar{o}}$: $\text{G}\bar{o}$ -typed Lennard-Jones potential, $\text{Solv}^{\text{G}\bar{o}}$: $\text{G}\bar{o}$ -typed potential with (de)-solvation effect, LJ^{ang} : Lennard-Jones potential with angular dependence, and Solv^{ang} : solvation potential with angular dependence. Each color curve represents the results of corresponding force fields, with homogeneous side-chain interaction: -0.1kcal/mol , single H_2O hydration: -0.5kcal/mol , temperature: 25°C , and integration step $\delta\theta = 10^{-4}$. Also, for visual comparison, the curves have been adjusted up/downward.

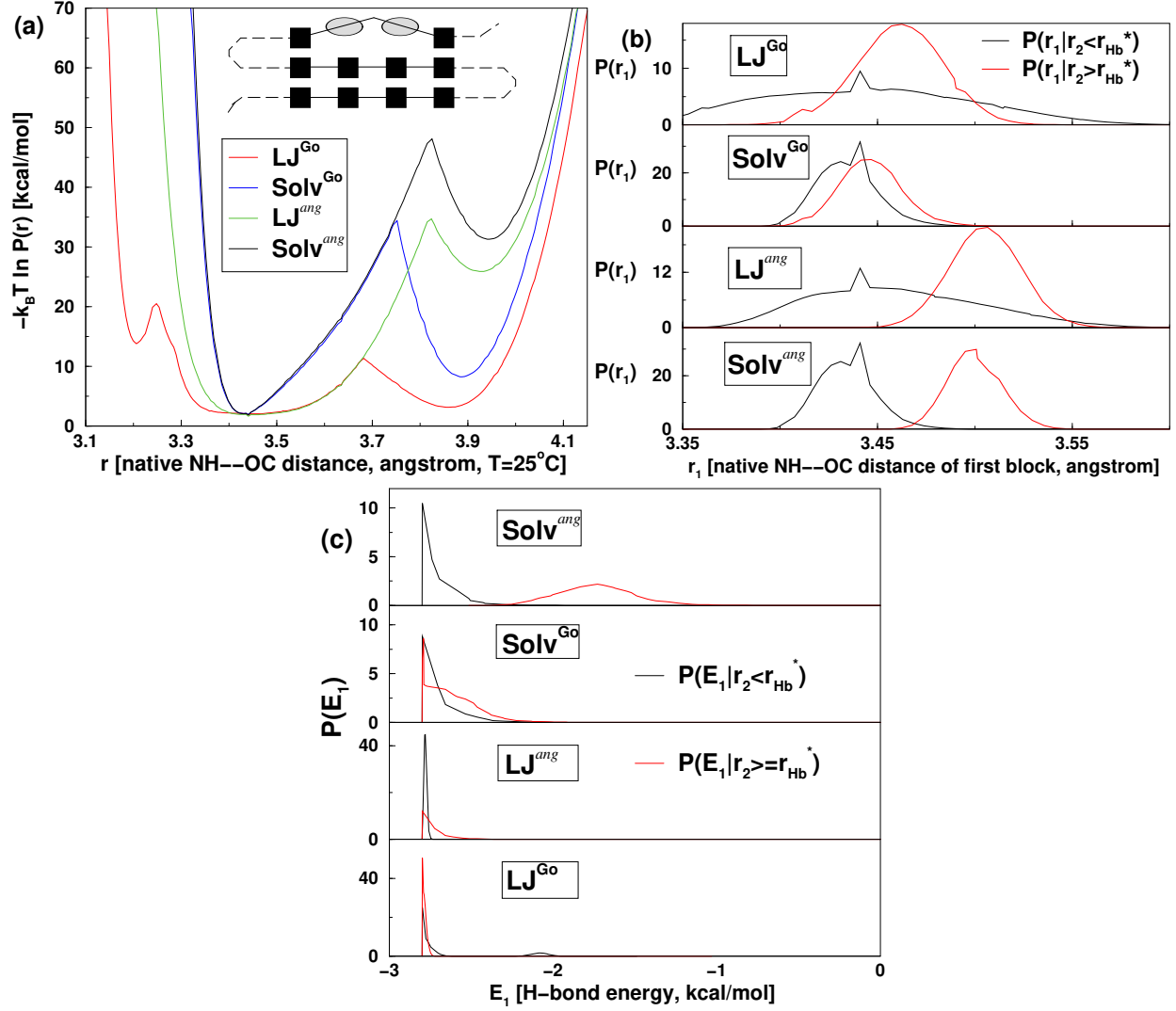


FIG. 4: The numerical results for buried two-block cases. **(a)** The pdf $P(r)$ for the native H-bond separation (average of the two symmetric mobile blocks). **(b)** The normalized conditional pdf in first molten block, $P(r_1)$, with respect to whether the second block is unfolded or folded (defined as if $r_2 \geq r_{\text{Hb}}^*$). Here r_1, r_2 are the H-bond separations of the two molten blocks with their native partner, respectively, and $\int dr_1 P(r_1|r_2 \geq r_{\text{Hb}}^*) = 1$. **(c)** The normalized conditional pdf in first molten block, $P(E_1)$, plotted on its H-bond energy E_1 .

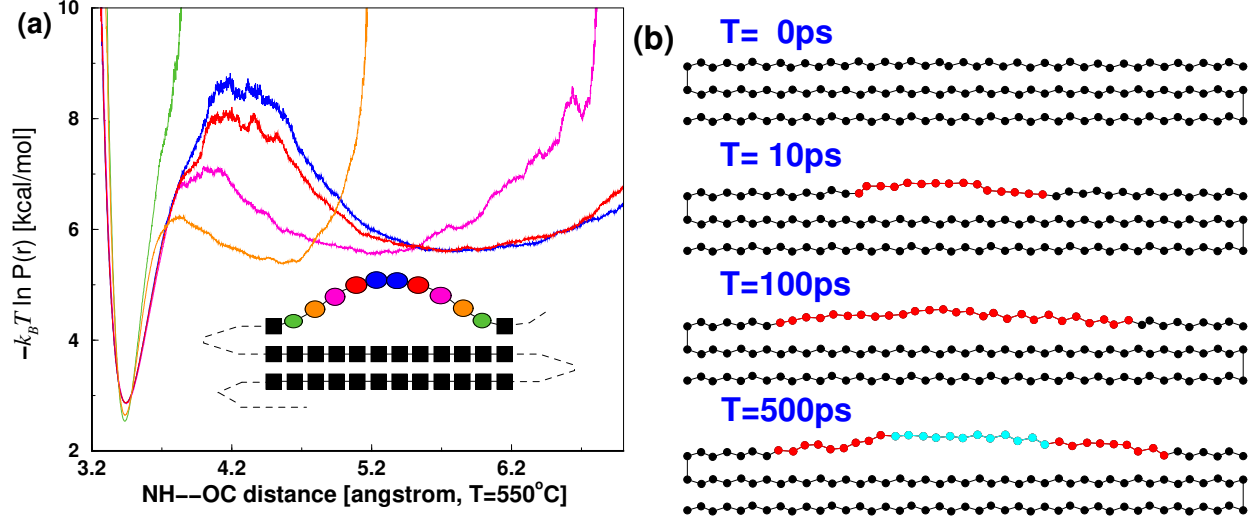


FIG. 5: (a): Langevin simulation results of a ten-block buried case. Each curve represents the corresponding block in the inset diagram, averaged over the symmetrical pair. Side-chain interaction: -0.1 kcal/mol. The simulation is averaged over 25 series of 1 ms runs ($\Delta t: 5 \times 10^{-5}$ ps). (b): snapshot of re-solvation simulation at $T = 850^\circ\text{K}$ where each heavy atom is labeled by different colors depending on the corresponding H-bond interacting distance r ($r < r_{\text{Hb}}^*$: black, $r_{\text{Hb}}^* \leq r < r_{\text{Hb}}^{\text{sol}}$: red, $r \geq r_{\text{Hb}}^{\text{sol}}$: cyan).